Investigating the linear viscoelastic behaviour at high frequencies in the transition to glassy regime for polystyrene melts and solutions

Zhong, Yiming; Yu, Liyun; Huang, Qian

Published in:
Rheologica Acta

Link to article, DOI:
10.1007/s00397-022-01359-8

Publication date:
2022

Document Version
Peer reviewed version

Investigating the linear viscoelastic behaviour at high frequencies in the transition to glassy regime for polystyrene melts and solutions

Yiming Zhong[1], Liyun Yu[2], Qian Huang[1,*]

[1]State Key Laboratory of Polymer Materials Engineering, Polymer Research Institute, Sichuan University, 610065 Chengdu, China
[2]Department of Chemical and Biochemical Engineering, Technical University of Denmark, 2800 Kongens Lyngby, Denmark

[*]qianhuang@scu.edu.cn

Abstract

This work focuses on the linear viscoelastic behaviour at length scales shorter than an entangled strand and attempts to connect it to the nonlinear behaviour (from data in literature) in fast extensional flow where such short length scales play an important role. We have measured the linear viscoelasticity at high frequencies in the transition to glassy regime for a series of polystyrene (PS) melts and solutions. When the samples are compared at the same T_{ref} -T_g, where T_{ref} is the reference temperature and T_g is the glass transition temperature, their third crossover points (near the glassy regime) of G' G'' plots are located at the same frequency. While the unentangled styrene oligomer behaves as a solvent in the flow and rubber plateau regimes, it contributes the same as the PS melts in the transition regime, unless the chain length is close to a Kuhn segment. In fast extensional flow, using τ_0 as the time scale and G_0 as the modulus scale, where τ_0 and G_0 are both associated with the third crossover point, the normalized steady-state extensional viscosity seems to depend on the number of Kuhn segments per chain, but not on the PS fraction. This is probably due to the contribution from the styrene oligomer solvent. However, fracture may happen before the steady state if the stretched polymer chains are close to their theoretical maximum stretch ratio.

Introduction

The difference of nonlinear rheology in extensional flow between polymer melts and solutions has been an active research topic especially during the last 10 years. With the same number of entanglements per chain, model linear polystyrene (PS) solutions show more strain hardening than the corresponding melts in transient extensional flow; their steady-state extensional viscosity also changes from extensional rate thinning to thickening with decreasing the polymer fractions (Huang et al. 2015). A key concept which may explain this difference is the so-called flow induced reduction of segmental friction. It says that when the Kuhn segments are aligned in fast extensional flow, the friction coefficient between chain segments decreases, while conventionally it is assumed to be constant. Details of this concept are summarized in a recent perspective by Ianniruberto et al. 2020 and a review by Matsumiya and Watanabe 2021. Although the reduction of friction is difficult to be measured directly in experiments and there are other explanations which can describe the above difference as well (e.g. Narimissa et al. 2019), it draws our attention to the fact that the length scales from a Kuhn segment to an entangled strand have important relations to the difference between polymer melts and solutions. This motivates our attempt in this work to find more information on such length scales from linear viscoelasticity.

As mentioned in the classical polymer physics book by Rubinstein and Colby 2003, the three crossover points in the plots of storage modulus G' and loss modulus G'' as a function of angular frequency ω for a linear entangled polymer melt divide the linear viscoelastic behaviour into four regimes, i.e. the flow regime, the rubber plateau regime, the transition regime, and the glassy regime. As shown in Fig.1, the first (at lower frequency) and second crossovers are related to the reptation time τ_d and entanglement relaxation time τ_e, respectively. The horizontal distance between these two crossover points scales with $Z^{3.4}$, where Z is the number of entanglements per chain. In most linear viscoelastic characterizations, measurements are performed using small amplitude oscillatory shear (SAOS) up to the frequency of the second crossover point, since the tube model parameters, i.e. Z, τ_e, and the plateau modulus G_N^0 can be found already in the first two regimes which are of most interest in linear rheology. While the first two regimes provide information mainly on the length scales from an entangled strand to the whole chain, the transition regime provides more information on length scales shorter than an entangled strand. For example, according to Rubinstein and Colby 2003, the third crossover point is related to the Kuhn segment relaxation time τ_0; The horizontal distance between the second and third crossover points (i.e. the ratio between τ_e and τ_0) scales with N_e^2 where N_e is the number of Kuhn segments per entangled strand, and the vertical distance (i.e. the ratio between G_0 and G_e, where G_0 and G_e are the modulus at the third and second crossover point, respectively) scales with N_e.

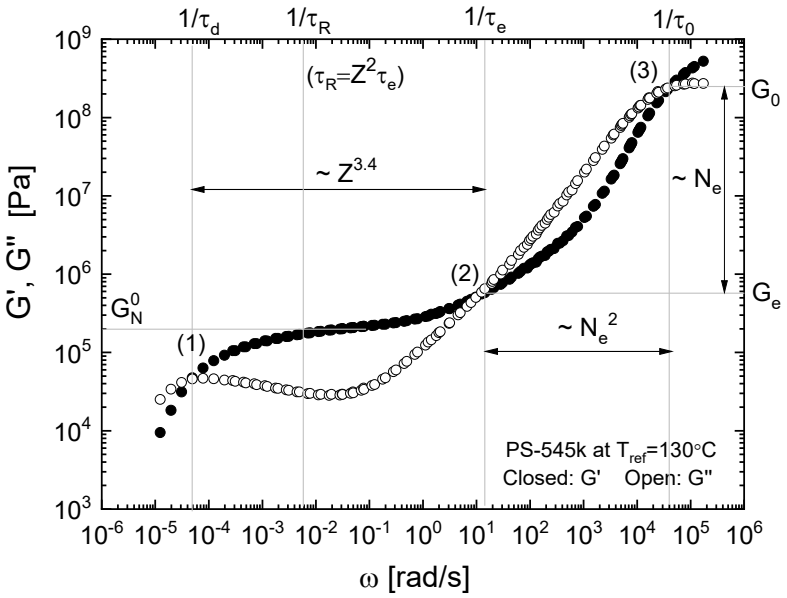

Fig.1 An example of a whole master curve (storage modulus G' and loss modulus G'' as a function of angular frequency ω) covering four regimes for a PS-545k melt at a reference temperature of 130°C.

In the work of Huang et al. 2015, the linear and nonlinear rheological data of PS melts and solutions are compared under normalization with their corresponding values of τ_e and G_N^0. In this way, their linear viscoelastic behaviour in the first two regimes is identical with each other, since all the samples have the same number of entanglements per chain Z. However, their linear viscoelastic behaviour in the transition regime would still be different since N_e is increasing with decreasing polymer fraction. Furthermore, Huang et al. 2013a showed that even with the same Z and N_e, PS solutions with different solvents (oligomeric styrene with different length) behave differently in extensional flow, although the flow rates are not fast enough to align the solvents. Huang et al. 2016 also showed that when liquid fracture happens, the local deformation rate near the crack tip is very fast - corresponding to the frequencies in the transition regime (i.e.

faster than $1/\tau_e$), while the flow rate $\dot{\epsilon}$ is much slower and corresponds to the rubber plateau regime ($1/\tau_R < \dot{\epsilon} < 1/\tau_e$). Therefore, characterization at higher frequencies in the transition to glassy regime is necessary. In literature there are several studies in the transition and glassy regimes (e.g., Inoue 2006; Larson 2004; Palade et al. 1996; Park et al. 2015), and the transition regime is often divided into the contribution from the high-frequency Rouse and the contribution from an empirical local segmental part (e.g., Majeste et al. 1998; Roland et al. 2004). However, to the best of our knowledge, there seems no systematic experimental investigation for polymer melts and their solutions.

In the present work, we measured the linear viscoelasticity in SAOS up to the frequency of the third crossover point for a series of PS melts and solutions. We checked if the scaling in Fig.1 holds for these samples, discussed the possible influence from the solvents, and re-compared the extensional steady-state viscosity and the liquid fracture data from literatures under normalization with parameters associated with the third crossover point.

Materials and Methods

The materials used in this study are PS melts and solutions as listed in Table 1 and 2, respectively. Most samples have been characterized in SAOS (at frequencies up to the second crossover point) as well as in uniaxial extensional flow in previous studies, and the corresponding references are also listed in the two tables. Most solutions use the oligomeric styrene OS-4k as the solvent. OS-4k has a molar mass of about 4000 g/mol which is far below the molar mass of an entangled strand (13300 g/mol as used in Huang et al. 2015). Details of sample preparation for these solutions can be found in Huang et al. 2015. Two extra solutions use shorter oligomers with molar mass of about 1000 g/mol and 500 g/mol, respectively. Sample preparations for these two solutions can be found in Huang et al. 2013a. In Table 2, some samples were prepared in different batches with slight differences in molecular weight and polymer fraction; these samples have been marked in the table and labelled according to the actual situation.

Table 1 Weight average molecular weight (M_w), dispersity (Đ), and glass transition temperature (T_g) of the polystyrene and oligomeric styrene (OS) melts

Sample Name	**Description**	**M_w** [g/mol]	**Đ**	**T_g** [ºC]	**Refs.**
PS-545k	Linear PS 545k	545000	1.12	106.5	Huang et al. 2013b
PS-285k	Linear PS 285k	285000	1.09	107.5	Huang et al. 2013b; Huang 2019
PS-185k	Linear PS 185k	185000	1.03	-	Huang et al. 2019
PS-Commercial	Commercial Linear PS	230000	3.83	100.5*	Huang and Rasmussen 2019
PS-Ring-185k	Ring PS 185k	185000	1.01	-	Huang et al. 2019
OS-4k	Linear OS 4k	4330	1.04	83.7*	Huang et al. 2015

*Re-measured in this work.

Table 2 Components and glass transition temperature of the linear polystyrene (PS) solutions

Sample Name	**Components**	**ϕ** [wt % of PS]	**T_g** [ºC]	**Refs.**
PS-545k/4k-70	545k + 4k	70 ± 1	101.0	Huang and Rasmussen 2017
PS-545k/4k-52 PS-545k/4k-48*	545k + 4k	52 ± 1	98.6	Huang et al. 2013a
PS-545k/4k-28	545k + 4k	28 ± 1	91.2	Huang and Rasmussen 2017

PS-576k/4k-26*				
PS-576k/4k-17	576k + 4k	17 ± 1	89.0	Huang 2019
PS-900k/4k-33 PS-864k/4k-33*	900k + 4k	33 ± 1	92.1	Huang et al. 2015
PS-1760k/4k-18	1760k + 4k	18 ± 1	89.0	Huang et al. 2015
PS-900k/4k-17 PS-864k/4k-17*	900k + 4k	17 ± 1	89.0	Huang and Rasmussen 2017
PS-545k/1k-52	545k + 1k	52 ± 1	54.0	Huang et al. 2013a
PS-545k/0.5k-52	545k + 0.5k	52 ± 1	-	-

*The second batch has slight differences in molecular weight and polymer fraction, and is therefore labelled accordingly.

In the work of André et al. 2021, it has been mentioned that the glass transition temperatures of PS solutions using 9000 g/mol OS as the solvent can be well described by the Fox equation. As shown in Fig.2, the Fox equation can also describe the T_g of the PS solutions in Table 2 using OS-4k as the solvent. The T_g of the pure OS-4k was reported to be 76.5 ºC in Huang et al. 2013a, which seems too low compared with the prediction of Fox equation. However, as also mentioned in André et al. 2021, the presence of residual solvent may have an influence on T_g. We therefore dried the OS-4k at 65 ºC for two days and re-measured the sample by differential scanning calorimetry (DSC) with a heating/cooling rate of 10 K/min under an inert atmosphere. The re-measured T_g of OS-4k is 83.7 ºC (356.85K) as shown in Fig.2 and listed in Table 1.

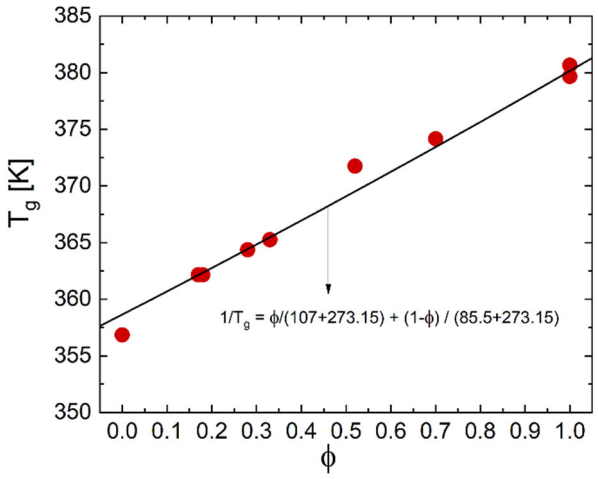

Fig.2 Glass transition temperatures T_g of the linear PS melts and solutions (using OS-4k as the solvent) as a function of weight fraction of the PS.

The SAOS measurements were carried out using an ARES-G2 rheometer from TA Instruments. A pair of parallel plates with diameters of either 8mm or 4mm were used depending on the magnitude of modulus. The 4mm plates are needed for high moduli to minimize the effect of instrument compliance as reported in Laukkanen 2017. Before the measurements, all the samples were dried in a vacuum oven at 40-60 ºC for 2-3 days. The measurements were performed at different temperatures ranging from T_g+5 ºC to T_g+100 ºC under nitrogen. For each sample, the data was shifted to a single master curve at a reference temperature T_{ref} using the time−temperature superposition (TTS) procedure. The van Gurp-Palmen plot, i.e. the phase angle δ vs. the complex modulus G^*, was made for each sample to check if TTS works, since this plot is affected by the modulus-shift factor b_T only, but not by the time-shift factor a_T. Figure 3 shows an example of the van Gurp-Palmen plot for the sample PS-545k/1k-52. The inset shows the modulus-shift factor b_T. The values of b_T

show an obvious change below 90 ºC, due to the change of sample density. The measurements at high moduli in the transition regime were performed at smaller amplitude to avoid wall slip. Smaller temperature steps, typically less than 5 ºC, were also used to get good TTS, as shown in Fig.3 for the data at $G^*>10^6$ Pa.

The three data points at δ=45º in Fig.3 correspond to the three crossover points in the plots of G', G'' vs. ω (e.g. Fig.1). In the rest of the work, we use the complex modulus G^* at the second and third crossover point as G_e and G_0 respectively, and G^* at the minimum δ in-between of the first and second crossover point as G_N^0, as marked in Fig.3.

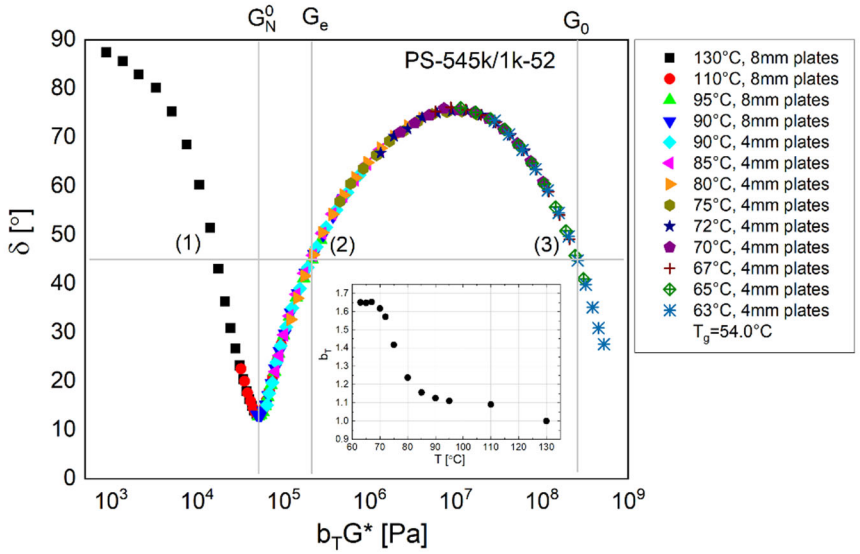

Fig.3 An example of van Gurp-Palmen plot (the phase angle as a function of the complex modulus) showing that TTS works well for the sample PS-545k/1k-52 in the temperature range from T_g+9 ºC to T_g+76 ºC. The inset shows the modulus-shift factor b_T.

Results

Master curves of G', G'' as a function of ω are first built at the reference temperature of T_0 = 130 ºC for all the samples. For linear PS melts with the same T_g (around 107 ºC), their master curves overlap each other nicely in the transition regime between the second and third crossover points as shown in Fig.4a, because these melts have the same number of Kuhn segments per entangled strand (N_e). The corresponding van Gurp-Palmen plots in Fig.4b show that the melts also have a similar G_N^0 of about 200kPa. Figure 4c and 4d compare the linear PS-185k with the ring PS that has the same molar mass and the unentangled OS-4k. Since the OS and ring PS melts cannot be entangled as the linear PS melts, they do not have the first and second crossover points which are associated with entanglements, but only have the third crossover point at high frequency. Furthermore, as shown in Table 1, OS-4k has a T_g much lower than the PS melts, thus its master curve at 130 ºC cannot be compared directly with the PS melts. Therefore, we shift the master curve of OS-4k (that originally built at T_0 = 130 ºC) to a new reference temperature T_{ref}, so that the third crossover point of OS-4k at T_{ref} locates at the same frequency as that of the PS melts at 130 ºC. In this way the two samples are compared under the same Kuhn segment relaxation time τ_0. The new T_{ref} for OS-4k is found to be 110 ºC and the corresponding master curve is plotted in Fig.4c. At high frequencies larger than 1000 rad/s, the master curves of the three melts also overlap each other nicely in Fig.4c, showing the same dynamics at short

length scales up to several Kuhn segments. Figure 4e and 4f show the moduli more clearly at the high-frequency regime for the samples in Fig.4a and 4c, respectively. The molar mass of one Kuhn segment for PS is M_0 =610 g/mol, leading to $N_e=M_e/M_0=21.8$ for entangled PS melts (using M_e=13300 g/mol) as reported in Huang et al. 2013b. For OS-4k it contains about 7 Kuhn segments per chain. In literature different values of M_e and M_0 have been reported for PS melts. For example, M_0 =833 g/mol and M_e =15000 g/mol are used in André et al. 2021. In this work the values are selected to be consistent with our previous works.

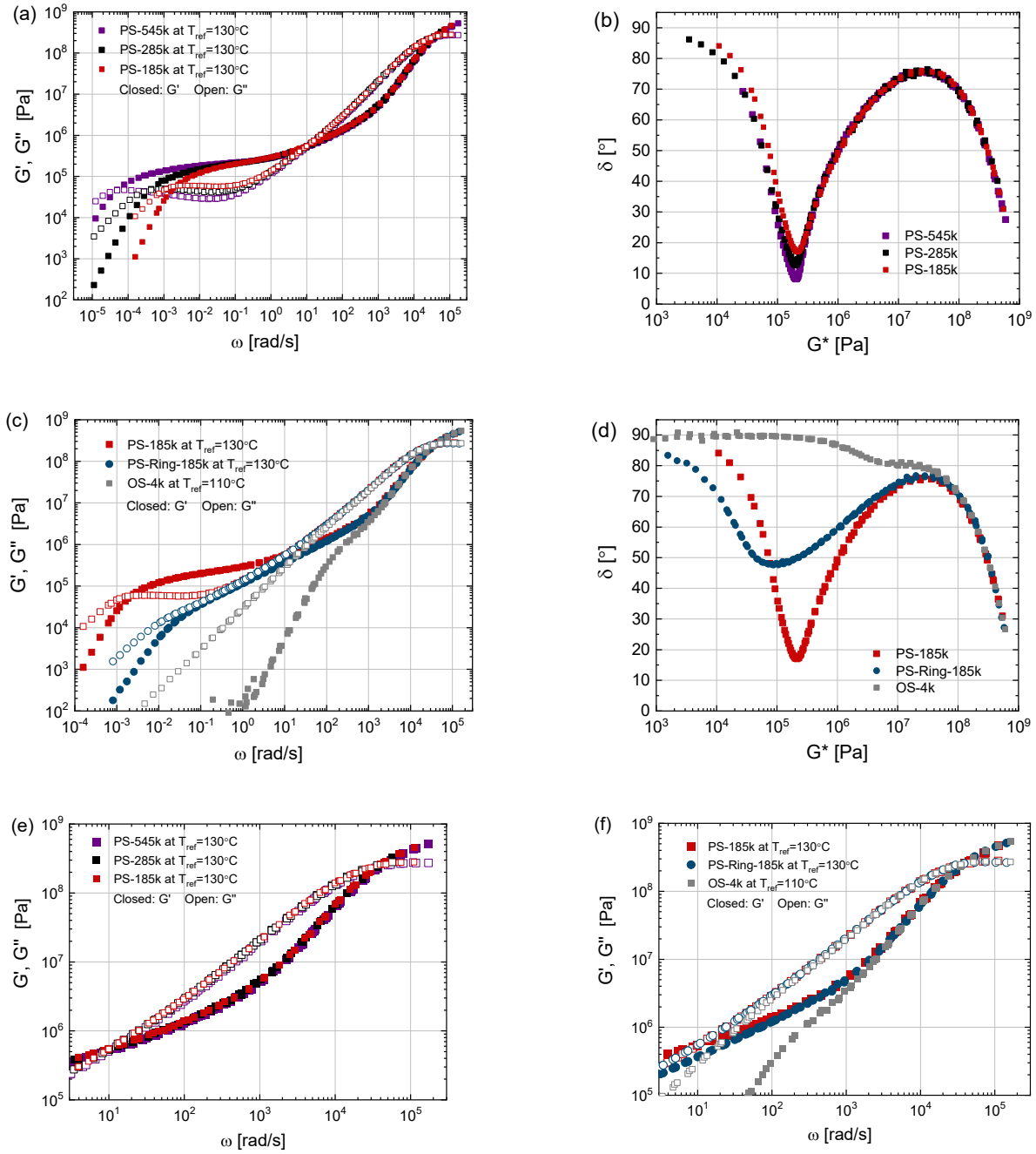

Fig.4 (a) The storage modulus G' and loss modulus G'' as a function of the angular frequency ω at reference temperatures T_{ref} (shown in the figure) for the linear entangled PS melts. (b) The van Gurp-Palmen plots (phase angle vs complex modulus) for the samples in Fig.4a. (c) Comparison of the storage modulus G' and loss modulus G'' as a function of the angular frequency ω for an entangled linear PS melt, a ring PS melt and an unentangled linear OS melt.

(d) The van Gurp-Palmen plots for the samples in Fig.4c. (e) The moduli at the high-frequency regime for the samples in Fig.4a. (f) The moduli at the high-frequency regime for the samples in Fig.4c. The data of PS-285k and OS-4k are taken from Huang 2019.

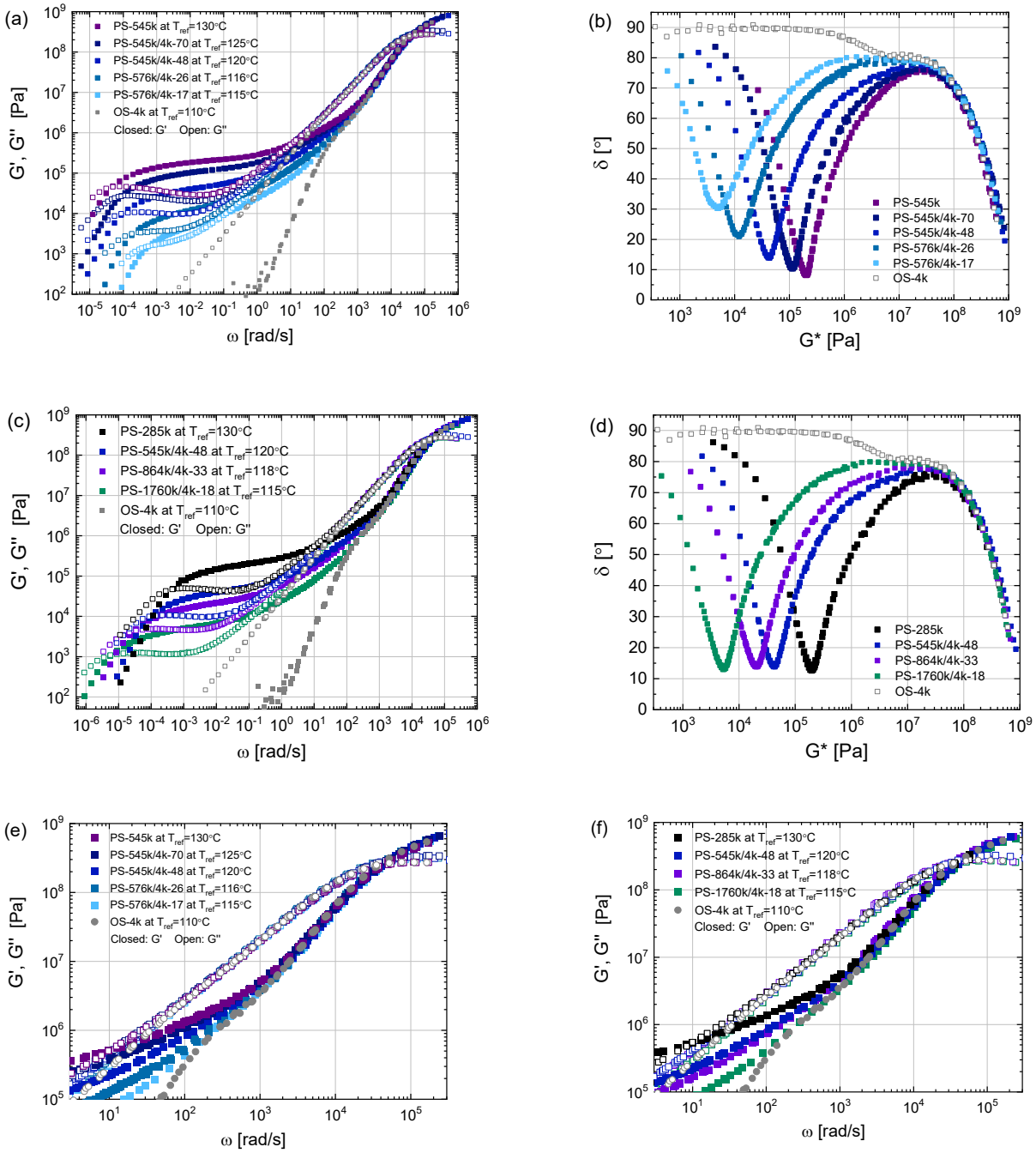

Fig.5 (a) The storage modulus G' and loss modulus G'' as a function of the angular frequency ω at reference temperatures T_{ref} for the linear PS melt PS-545k and its solutions at different concentrations. (b) The van Gurp-Palmen plots (phase angle vs complex modulus) for the samples in Fig.5a. (c) The storage modulus G' and loss modulus G'' as a function of the angular frequency ω at reference temperatures T_{ref} for the linear PS melt and solutions that have the similar number of entanglements per chain Z. (d) The van Gurp-Palmen plots for the samples in Fig.5c. (e) The moduli at the high-frequency regime for the samples in Fig.5a. (f) The moduli at the high-frequency regime for the samples in Fig.5c. The data of PS-864k/4k-33, PS-1760k/4k-18, and PS-576k/4k-17 are taken from Huang 2019.

Figure 5 compares the linear PS solutions using OS-4k as the solvent. The T_g of the PS solutions is decreasing with lower PS fractions; therefore, the master curves of all the solutions (that originally built at T_0 = 130 ºC) are again shifted to a new T_{ref} so that their third crossover points locate at the same frequency as that of the PS melts. The new T_{ref} for each sample is listed in Table 3. As already shown in Fig.4c, since the solvent OS-4k contains about 7 Kuhn segments per chain and has the same G' and G'' as the PS melts at high frequencies, the master curves of all the solutions in Fig.5 also overlap each other at high frequencies > 1000 rad/s (modulus > 10^7 Pa). Therefore, for these solutions, the OS-4k does *not* behave as a 'solvent' at high frequencies in the transition regime. It acts as a solvent only in the flow and plateau regimes of the solutions. Figure 5a and 5b compare the group of PS solutions with the same long chain (545kg/mol or 576 kg/mol) diluted in OS-4k with different PS fractions from 17% to 70%. Data of the pure long chain (PS-545k melt) and the pure solvent (OS-4k) are also included in the figures for comparison. Figure 5c and 5d compare another group of PS solutions that have the same number of entanglements per chain (Z≈22). As seen in Fig.5d, the minimum phase angle (at $G^*<10^6$ Pa) of the four samples is almost the same, showing that they have the same Z. By contrast, the minimum phase angle of the samples in Fig.5b increases with decreasing the PS fraction, showing that Z is decreasing. Figure 5e and 5f show the moduli more clearly at the high-frequency regime for the samples in Fig.5a and 5c, respectively.

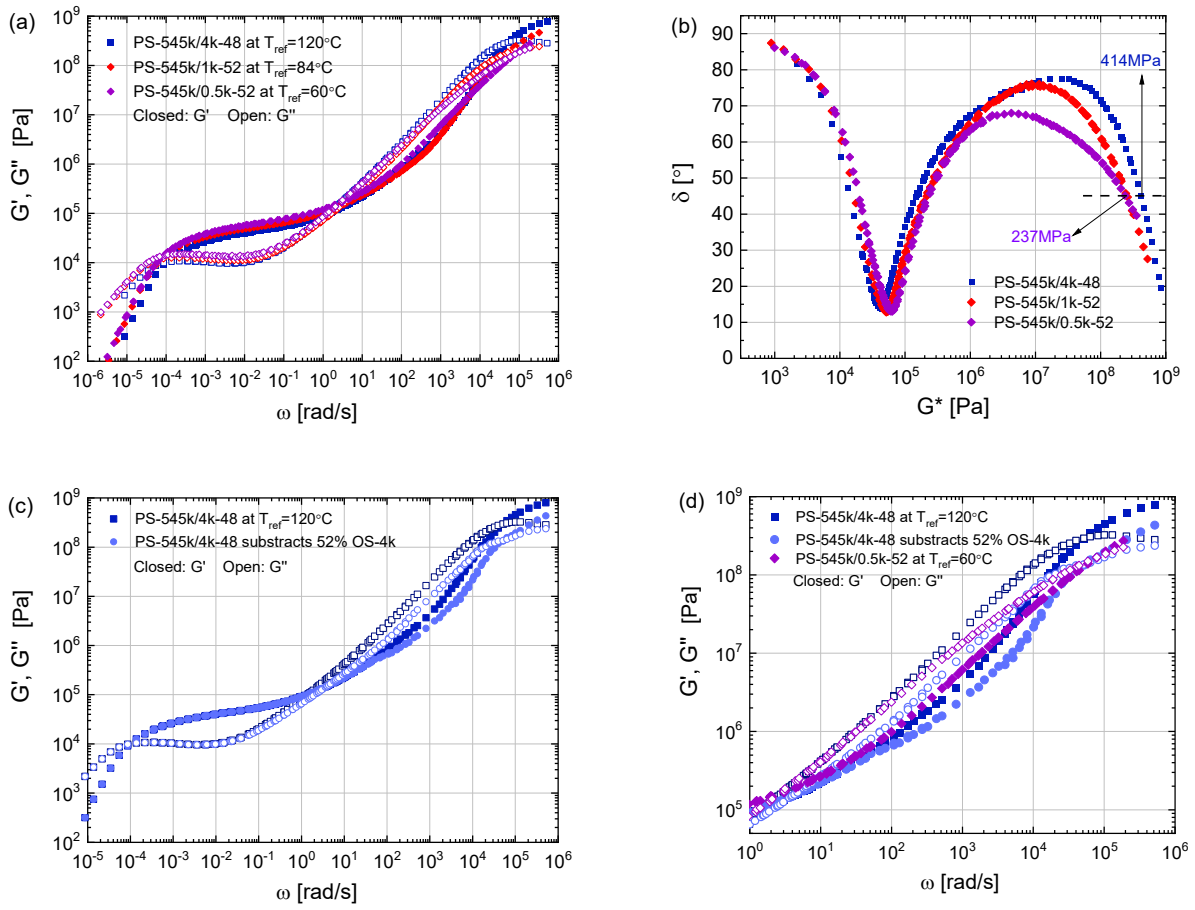

Fig.6 (a) The storage modulus G' and loss modulus G'' as a function of the angular frequency ω at reference temperatures T_{ref} for three PS-545k solutions with similar PS concentration (50%) but different solvents (oligomers). (b) The van Gurp-Palmen plots (phase angle vs complex modulus) for the samples in Fig.4a. (c) Comparison between the original and corrected G' and G'' as a function of ω for PS-545k/4k-48. (d) Comparison between the corrected data of PS-545k/4k-48 and the original data of PS-545k/0.5k-52 at high frequencies in the transition to glassy regime.

Figure 6 compares a special group of PS solutions containing the same PS (PS-545k) with a similar fraction ($\varphi \approx 50\%$) but using different oligomeric styrene with molar mass of 500g/mol (OS-0.5k), 1000g/mol (OS-1k), and 4000 g/mol (OS-4k), respectively. The solutions are also compared under different T_{ref} where their third crossover points are located at the same frequency as mentioned before. While OS-4k has 7 Kuhn segments per chain, OS-1k contains only 1.6 Kuhn segments, and OS-0.5k is even shorter than one Kuhn segment. Therefore, the latter two are much closer to a 'real' isotropic solvent. In contrast to the situation in Fig.5, Fig.6a shows that the master curves of the three solutions do not overlap each other at high frequencies in the transition regime. The difference is clearer in the van Gurp-Palmen plots at $G^* > 10^6$ Pa in Fig.6b. The phase angle of the solution PS-545k/0.5k-52, using OS-0.5k as the solvent, is obviously smaller than the other two, indicating less dispassion of this sample in the transition regime. Furthermore, while the modulus at the third crossover point (G_0) is the same for all the solutions in Fig.5 and equals the value of the melts ($G_0=G_{0m}$), the value of G_0 for PS-545k/0.5k-52 is approximately ϕG_{0m}, where ϕ is the weight fraction of the PS. This also shows that OS-0.5k behaves as a solvent also at high frequencies in the transition regime, in contrast to OS-4k. Figure 6c compares the original data of PS-545k/4k-48 with the corrected data by simply subtracting 52% OS-4k, i.e., $G'_{corrected} = G'_{original} - 0.52G'_{OS\text{-}4k}$ and $G''_{corrected} = G''_{original} - 0.52G''_{OS\text{-}4k}$. The data at the flow and rubber plateau regimes are almost not affected, but there is an obvious change in the transition regime. The horizontal positions of the second and third crossover points only have a small shift. In Fig.6d we compare the corrected data of PS-545k/4k-48 with the original data of PS-545k/0.5k-52 in the transition regime. The two data sets do not agree with each other entirely, but the third crossover points overlap. We use the original data sets of the PS solutions for analysis in the rest of the paper.

Table 3 Material parameters for all the PS melts and solutions investigated

Sample Name	**Z**	**N_e**	**T_{ref}** [°C]	**τ_d** [s]	**τ_e** [s]	**τ_0** [ms]	**G_N^0** [kPa]	**G_e** [kPa]	**G_0** [MPa]
PS-545k	41.0	21.8	130	20300	0.103	0.0199	201	716	358
PS-285k	21.4	21.8	130	2250	0.100	0.0223	197	763	395
PS-185k	13.9	21.8	130	451	0.100	0.0253	215	777	367
PS-Commercial	-	-	127	1490	0.101	0.0212	145	695	379
PS-Ring-185k	-	-	130	-	-	0.0259	-	-	363
OS-4k	-	-	110	-	-	0.0229	-	-	373
PS-545k/4k-70	28.7	31.1	125	11400	0.210	0.0194	111	409	421
PS-545k/4k-48	19.7	45.4	120	9800	0.647	0.0193	43.6	151	414
PS-576k/4k-26	11.3	83.8	116	4410	3.14	0.0199	12.0	39.2	426
PS-576k/4k-17	7.4	128.2	115	1630	8.54	0.0207	4.84	14.2	385
PS-864k/4k-33	21.4	66.1	118	36100	1.49	0.0254	21.3	74.4	382
PS-1760k/4k-18	23.8	121.1	115	178000	5.54	0.0209	5.18	18.4	371
PS-864k/4k-17	11.0	128.2	115	9790	6.44	0.0202	4.54	17.1	410
PS-545k/1k-52	21.3	41.9	84	14000	0.303	0.0195	51.6	215	260
PS-545k/0.5k-52	21.3	41.9	60	12100	0.329	0.0170	60.3	241	237

In Table 3, we summarize the parameters for all the samples. The characteristic times of τ_d, τ_e, and τ_0 are obtained directly from the three crossover points respectively, as illustrated in Fig.1. The moduli G_N^0, G_e, and G_0 are obtained from the van Gurp-Palmen plots as illustrated in Fig.3. The number of entanglements per chain for linear PS systems is simply calculated as $Z=M_w/M_e$, where M_w is the weight average molar mass of the PS chain and M_e is the molar mass of one entangled strand. For PS solutions, we use $M_e=13300\phi^{-1}$ g/mol where ϕ is the PS fraction. For PS melts, $\phi=1$. The number of Kuhn segments per entangled strand is thus calculated as $N_e=21.8\phi^{-1}$.

Discussions

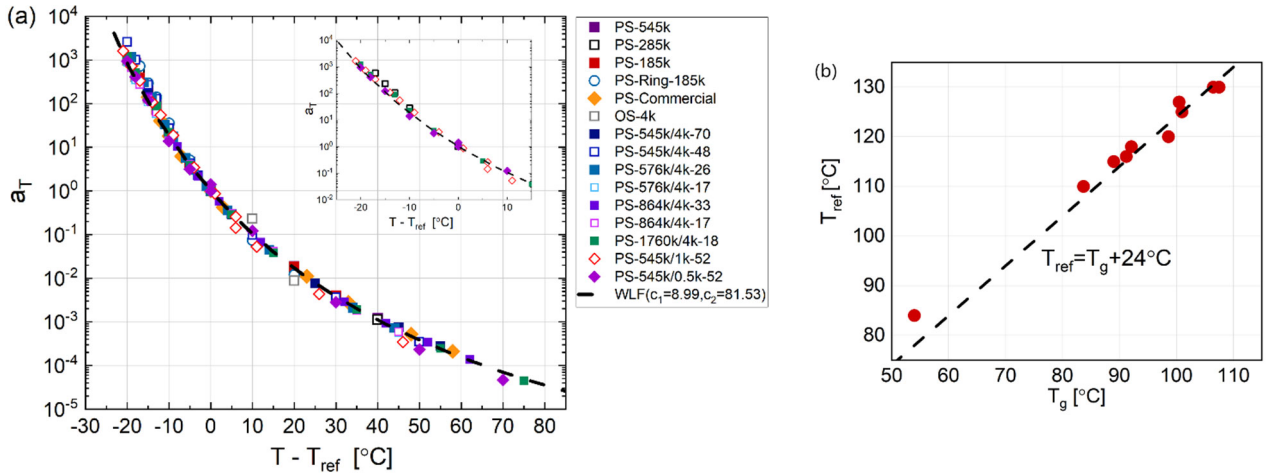

Fig.7 (a) The time-temperature shift factors a_T as a function of T-T_{ref} for all the PS melts and solutions. The dashed line is the calculation from Williams−Landel−Ferry (WLF) equation using c_1=8.99, c_2=81.53 K, and T_0 = 130 °C as reported in Huang et al. 2015. The inset shows a clearer picture at low temperatures for less samples. (b) The reference temperature T_{ref} (listed in Table 3) of each sample as a function of their corresponding glass transition temperature T_g measured from DSC (listed in Table 1 and 2)

As mentioned in the section above, the PS melts and solutions are compared at a reference temperature T_{ref}. It should be noted that in the step of determining T_{ref}, we did *not* use T_g which was measured from DSC, because several factors, such as the heating/cooling rate and the broadness of the DSC trace at the transition, influence the T_g values obtained from DSC. The rheological data is more sensitive to T_g, and here the reference temperature T_{ref} for each sample was found by shifting the third crossover points of all the samples to the same frequency, so that the samples are compared under exactly the same Kuhn segment relaxation time τ_0. In Fig.7a, we plot the time-temperature shift factor a_T as a function of T-T_{ref}. The data of all the samples form a nice master curve, showing that they have the same temperature dependence from T_{ref}. As shown in the dashed line in the figure, this master curve can be well described by the Williams−Landel−Ferry (WLF) equation

$$\log_{10} a_T = \frac{-c_1(T - T_0)}{c_2 + (T - T_0)},$$

where c_1=8.99, c_2=81.53 K, and T_0 = 130 °C as reported in Huang et al. 2015 for PS melts. Although the values of c_1 and c_2 in Huang et al. 2015 were obtained by fitting the data measured from T_0 (130°C) and above, it seems that the calculated result in Fig.7a also matches the data at lower temperatures down to T_{ref} - 20°C. Figure 7b compares the T_{ref} of each sample with their corresponding T_g measured from DSC. It is found that T_{ref} is approximately at the same distance from T_g, i.e. T_{ref} -T_g ≈ 24°C. This confirms that comparing the results at the same T_{ref}-T_g, as performed in the work by e.g. Shahid et al. 2019 and André et al. 2021, is equivalent as comparing the results with their third crossover points locating at the same frequency. In other words, the samples are compared based on the same τ_0.

We next check if the scaling of the characteristic times and moduli, as illustrated in Fig.1, still holds for the investigated samples. This is of particular interest for the solutions using OS-4k as the solvent, since we have

mentioned that OS-4k acts as a solvent only in the flow and plateau regimes but not at high frequencies in the transition regime. Figure 8a plots G_N^0 and G_e as a function of the PS fraction ϕ. Here both G_N^0 and G_e scale with ϕ^2 in Fig.8a, which agrees with the observations reported in Huang et al. 2013b, 2015. At lower PS concentrations, the scaling of G_N^0 has a transition from ϕ^2 to $\phi^{2.33}$ due to an enhanced contour length fluctuation process as analysed in detail by Shahid et al. 2017. The data points at ϕ<0.2 in Fig.8a also show some deviation from the ϕ^2 scaling, but the deviation is small. Since $G_N^0 = \rho\phi RT/ M_e$, the ϕ^2 scaling confirms that M_e (or N_e) ~ ϕ^{-1} (as calculated in Table 3) holds for all the samples investigated. Figure 8b plots the ratio of G_e and G_0 as a function of ϕ. As illustrated in Fig.1, the distance between G_0 and G_e is expected to scale with N_e according to Rubinstein and Colby 2003. Therefore, with N_e scales with ϕ^{-1}, G_e/G_0 is expected to scale with ϕ. However, due to the influence of OS-4k in the transition regime, it is found in Fig.8b that G_e/G_0 scales with $\phi^{1+\alpha}$ instead, where α is between 1 and 4/3. Figure 9 checks the scaling of the characteristic times. As expected, the ratio of τ_d and τ_e scales approximately with $Z^{3.4}$ as shown in Fig.9a. At Z<10 there is an obvious deviation; As reported by Shahid et al. 2017, the scaling may change from $Z^{3.4}$ to Z^4 at lower Z values also due to the enhanced fluctuation process. The ratio of τ_e and τ_0 is expected to scale with N_e^2 as illustrated in Fig.1, but again due the influence of OS-4k, in Fig.9b it is found to scale with $N_e^{2.33}$.

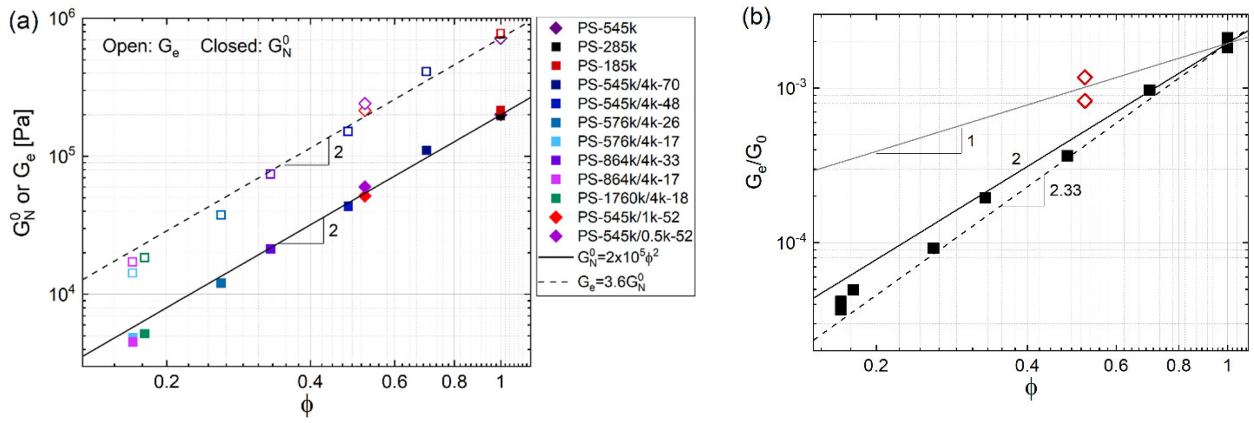

Fig.8 (a) The plateau modulus G_N^0 and the modulus at the second crossover point G_e as a function of PS fraction ϕ. (b) The ratio of the muduli at the second and third crossover point as a function of PS fraction ϕ; The closed symbols are for melts and solutions using OS-4k as the solvent, while the open symbols are for the two extra solutions using OS-1k and OS-0.5k as the solvent.

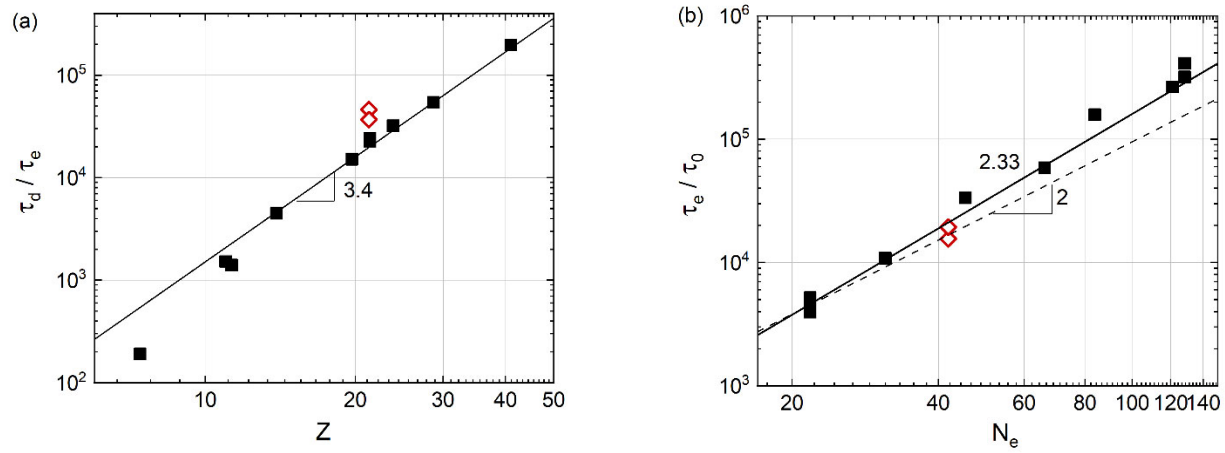

Fig.9 (a) The ratio of reptation time τ_d and entanglement relaxation time τ_e as a function of the number of entanglements per chain Z. (b) The ratio of entanglement relaxation time τ_e and Kuhn segement relaxation time τ_0 as a function of the number of Kuhn segements per entangled strand N_e. The closed symbols are for melts and solutions using OS-4k as the solvent, while the open symbols are for the two extra solutions using OS-1k and OS-0.5k as the solvent.

Finally, we look at the nonlinear rheological data in extensional flow from literature for the PS melts and solutions. As reported by André et al. 2021, for polymer solutions using 9kg/mol OS as the solvent, the measured extensional steady-state viscosity at fast stretch rates scales with $\phi^{0.5}$. However, this is not expected by classical theories as also mentioned by André et al. 2021: according to theories, the steady stress at fast rates scales with $G_N^0 \lambda^2$ where λ is the chain stretch ratio; Since λ scales with $N_e^{0.5}$ (thus $\phi^{-0.5}$) and G_N^0 scales with ϕ^2, the steady stress is therefore expected to scale with ϕ, instead of the observed $\phi^{0.5}$. In Fig.10a, we plot the normalized extensional steady-state viscosity of the PS melts and solutions (using OS-4k as the solvent) as a function of Rouse time ($\tau_R = Z^2\tau_e$) based Weissenberg number, following the same way as in Fig.16 of André et al. 2021. The extensional data are taken from references listed in Table 1 and 2. Some PS solutions using OS-9k as the solvent, taken from André et al. 2021, are also included in Fig.10a for comparison. It should be noted that in André et al. 2021, the relaxation time τ_e is not estimated the same way as in this work (in this work we simply take the inverse of the second cross-over frequency as shown in Fig.1) and is thus about 5 times larger than that in this work. The values of M_e and G_N^0 in André et al. 2021 are also slightly different from the values used in this work. In order to compare with the OS-4k solutions, the data of the OS-9k solutions in Fig.10a have been re-calculated according to the parameters used in this work. In addition, the extensional data of two PS blends, PS-545k/285k-10 and PS-545k/285k-50 taken from Huang 2013, are plotted in Fig.10a as well. The Rouse time of the blends is calculated according to Eq.13 in André et al. 2021. It seems that for all the samples in Fig.10a, the data in fast flow approximately follow the $\phi^{0.5}$ scaling as mentioned in André et al. 2021. However, if we normalize the same extensional data with G_0 instead of $G^0_{Nmelt}\,\phi^{0.5}$ as shown in Fig.10b, we get a similar figure or even slightly better when compared with the envelope shown as the grey solid line in both figures. Since G^0_{Nmelt} is a constant (G^0_{Nmelt}=200kPa is used in Fig.10a for all the samples) and G_0 of the OS-4k solutions is also a constant (G_0=400MPa is used in Fig.10b; for OS-9k solutions G_0 is assumed to be 400MPa as well), the only difference between Fig.10a and 10b is the $\phi^{0.5}$. Fig.10b indicates that the steady-state viscosity of the samples is not related to ϕ in fast extensional flow, which is probably due to the contribution of the anisotropic solvents to extensional stress. When the flow is fast enough to align the Kuhn segments (i.e. faster than $1/\tau_R$) of the polymer chains, the length scales shorter than an entangled strand start to play a more important role. Although the flow is not fast enough to align the solvent molecules (compared with the corresponding Rouse time of the pure solvents), the short oligomeric chains are still possible to be aligned by the long polymer chains as mentioned in Huang et al. 2013a. As OS-4k contributes the same as the PS melts at short length scales, the data is finally not related to ϕ. Furthermore, at this stage the molecular friction should also be the same for all the samples, but it does not necessarily equal to the friction at equilibrium; in other words, the independence of ϕ cannot rule out the existence of friction reduction.

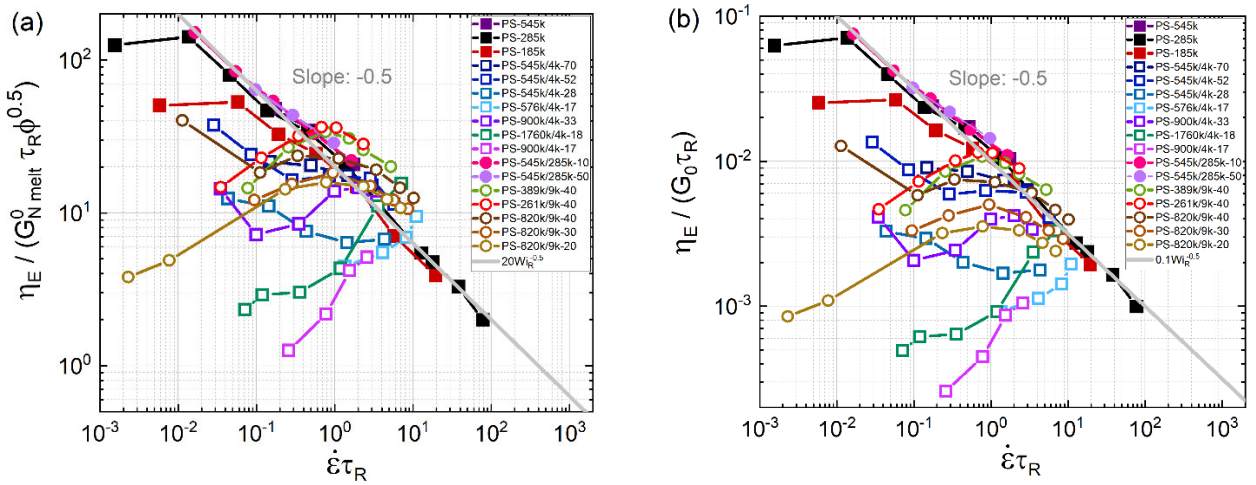

Fig.10 (a) The normalized steady-state extensional viscosity as a function of Rouse time (τ_R) based Weissenberg number following the same way as Fig.16 of André et al. 2021. G^0_{Nmelt} = 200 kPa is used for all the samples here. (b) The steady-state extensional viscosity normalized with G_0 and τ_R as a function of τ_R based Weissenberg number. G_0 = 400 MPa is used for all the samples here. The extensional data of the two PS-545k/285k blends are taken from Huang 2013; the OS-9k solutions are taken from André et al. 2021; the rest samples are taken from the references listed in Table 1 and 2. For calculating the Rouse time ($Z^2\tau_e$), τ_e is estimated according to Fig.1.

In addition to steady-state viscosity, we further include the data of extensional stress growth coefficient at fracture (taken from Huang 2019) in Fig.11 since fracture may happen before steady state in fast flows. Note that τ_R (calculated as $Z^2\tau_e$ in Fig.10) has been replaced with $N^2\tau_0$ in Fig.11. Since τ_e/τ_0 scales approximately with N_e^2 (more exactly should be $N_e^{2.33}$ for the OS-4k solutions, but the deviation is small), τ_R scales approximately with $N^2\tau_0$ (where $N=ZN_e$). We choose $N^2\tau_0$ here, because τ_0 is a constant (as shown in Table 3) when the samples are measured at T_{ref} where T_{ref}-T_g is the same (as shown in Fig.7b). The value of τ_0 for the OS-9k solutions is not reported in André et al. 2021; but the extensional data is measured at $T_{ref}=T_g+23.4°C$ which is similar with the case in Table 3 (where $T_{ref} \approx T_g+24°C$ as shown in Fig.7b). Therefore τ_0=0.02ms (as reported in Table 3) is used for the OS-9k solutions. The extensional stress at fracture for the PS-285k melt is found to be well described by $\sigma_E=3G_e\lambda^2_{max}$, where $\lambda_{max}=N_e^{0.5}$ is the theoretical maximum chain stretch ratio. The black solid line in Fig.11 shows the corresponding η_E (normalized by G_0 and $N^2\tau_0$) for PS melts where λ_{max} is reached, while the dash-dot and dash lines are for the PS solutions with PS fraction of 0.5 and 0.17 respectively, using $G_e \sim \phi^2$ and $\lambda_{max} \sim \phi^{-0.5}$. Hence the grey area in Fig.11 shows the regime where the theoretical λ_{max} is reached for the samples with ϕ from 0.17 to 1. Figure 11 shows that in fast extensional flow, the steady-state viscosities have the same envelope as shown in the grey solid line with the -0.5 slope (which can also be seen in Fig.10b); therefore the steady-state viscosities are dependent on the total number of Kuhn segments per chain N (since it influences the Rouse time) but not on ϕ. However, before reaching the grey solid line, if the stretched polymer chains are already close to their theoretical λ_{max} (i.e., the part of the grey regime which is under the grey solid line), fracture happens before steady state. The solution using OS-1k as the solvent seems to behave differently, but the available data is very limited. We also tried to include the data of PS solutions using isotropic small molecules as reported in Bhattacharjee et al. 2002; however, all the available data end before reaching the maximum chain stretch limit or the steady-state envelope, so their behaviour at higher rates is still unclear. In Fig.11 we only put one of these samples as an example (where G_0 and τ_0 are estimated according to the scaling in this work). In addition, while the results of simulations reported by O'Connor et al. 2018 also show that the normalized steady-state viscosity of

different samples approaches to the same value at high stretch rates, the situation of fracture is not considered there.

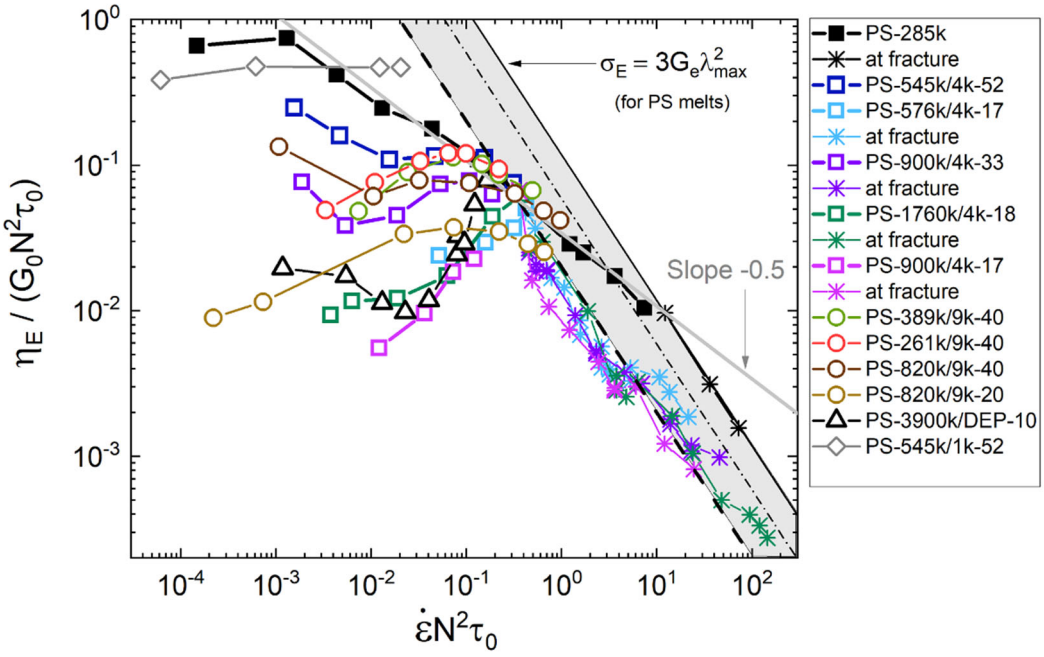

Fig.11 The normalized steady-state extensional viscosity, or extensional stress growth coefficient at fracture (if fracture happens before steady state), as a function of normalized stretch rate, using G_0 as the modulus scale and $N^2\tau_0$ as the time scale. N is the total number of Kuhn segments per chain, i.e. $N=ZN_e$. The extensional data of PS-3900k/DEP-10 is taken from Bhattacharjee et al. 2002; the OS-9k solutions are taken from André et al. 2021; the rest samples are taken from the references listed in Table 1 and 2.

Conclusions

We have systematically studied the linear viscoelastic behaviour at high frequencies in the transition to glassy regime for a series of PS melts and solutions. We confirm that the time-temperature superposition works well in this regime, and the shift factors can be well described by the same WLF equation which was obtained from the measurements in the flow and rubber plateau regimes. All the samples are compared at a reference temperature T_{ref}, where T_{ref} is selected in a way that the third crossover points of G' G'' for all the samples are located at the same frequency (i.e., the samples have the same Kuhn segment relaxation time τ_0). Styrene oligomer solvents with different molar mass have obvious influence on the solutions in the transition regime, but not in the flow and rubber plateau regimes. The solutions using OS-4k (which contains about 7 Kuhn segments) as the solvent have the same G_0 with that of the melts, while the solutions using oligomers shorter than 2 Kuhn segments have a lower G_0. For the melts and solutions using OS-4k or OS-9k as the solvent, their steady-state extensional viscosity in fast extensional flow seems related to the length of the PS chain only (i.e., the number of Kuhn segments of the whole chain, N), but not related to ϕ. This is probably due to the contribution of the oligomeric solvents which have the possibility to be aligned and become anisotropic. However, fracture may happen before the steady state if the stretched polymer chains are close to their theoretical maximum stretch ratio. The solution using OS-1k as the solvent seems to have a different behaviour, but the data is limited for a further investigation. This work shows that the length scales shorter

than an entangled strand play an important role in extensional flow. The contribution to extensional stress from the oligomeric solvents with more than 2 Kuhn segments cannot be ignored, and thus the samples should be considered as a ‘blend’ rather than a ‘solution’ in fast extensional flow. It would be interesting to further investigate such linear and nonlinear behaviour for solutions with isotropic solvents, pure oligomers with different Kuhn segements, as well as entangled melts with different chemistry.

Acknowledgement Financial support from the State Key Laboratory of Polymer Materials Engineering (Grant No. sklpme2020-1-04）and the National Natural Science Foundation of China (Grant No. 52173022) is gratefully acknowledged

References

André A, Shahid T, Oosterlinck F, Clasen C, van Ruymbeke E (2021) Investigating the Transition between Polymer Melts and Solutions in Nonlinear Elongational Flow. Macromolecules 54: 2797-2810.

Bhattacharjee PK, Oberhauser JP, McKinley GH, Leal LG, Sridhar T (2002) Extensional Rheometry of Entangled Solutions. Macromolecules 35: 10131-10148.

Huang Q (2019) Exploring the mechanism of fracture for entangled polymer liquids in extensional flow. Physics of Fluids 31: 083105.

Huang Q, Rasmussen HK (2019) Extensional flow dynamics of polystyrene melt. Journal of Rheology 63: 829-835.

Huang Q, Ahn J, Parisi D, Chang T, Hassager O, Panyukov S, Rubinstein M, Vlassopoulos D (2019) Unexpected Stretching of Entangled Ring Macromolecules. Physical Review Letters 122: 208001.

Huang Q, Rasmussen HK (2017) The transition between undiluted and oligomer-diluted states of nearly monodisperse polystyrenes in extensional flow. Rheologica Acta 56: 719-727.

Huang Q, Alvarez NJ, Shabbir A, Hassager O (2016) Multiple cracks propagate simultaneously in polymer liquids in tension. Physical Review Letters 117: 087801.

Huang Q, Hengeller L, Alvarez NJ, Hassager O (2015) Bridging the Gap between Polymer Melts and Solutions in Extensional Rheology. Macromolecules 48: 4158-4163.

Huang Q (2013) Molecular rheology of complex fluids, PhD thesis, Technical University of Denmark.

Huang Q, Alvarez NJ, Matsumiya Y, Rasmussen HK, Watanabe H, Hassager O (2013a) Extensional Rheology of Entangled Polystyrene Solutions Suggests Importance of Nematic Interactions. ACS Macro Letters 2: 741-744.

Huang Q, Mednova O, Rasmussen HK, Alvarez NJ, Skov AL, Almdal K, Hassager O (2013b) Concentrated Polymer Solutions are Different from Melts: Role of Entanglement Molecular Weight. Macromolecules 46: 5026-5035.

Ianniruberto G, Marrucci G, Masubuchi Y (2020) Melts of linear polymers in fast flows. Macromolecules 53: 5023−5033.

Inoue T (2006) On the Relationship between Viscoelastic Segments and Kuhn Segments; Strain-Induced Chain Orientation in Fast Deformation. Macromolecules 39: 4615-4618.

Larson RG (2004) An Explanation for the High-Frequency Elastic Response of Dilute Polymer Solutions. Macromolecules 37: 5110-5114.

Laukkanen O-V (2017) Small-diameter parallel plate rheometry: a simple technique for measuring rheological properties of glass-forming liquids in shear. Rheologica Acta: 56: 661-671.

Majeste J-C, Montfort J-P, Allal A, Marin G (1998) Viscoelasticity of low molecular weight polymers and the transition to the entangled regime. Rheologica Acta 37 :486-499.

Matsumiya Y, Watanabe H (2021) Non-universal features in uniaxially extensional rheology of linear

polymer melts and concentrated solutions: A review. Progress in Polymer Science 112: 101325.
Narimissa E, Huang Q, Wagner MH (2019) Elongational rheology of polystyrene melts and solutions: Concentration dependence of the interchain tube pressure effect. Journal of Rheology 64: 95-110.
O'Connor TC, Alvarez NJ, Robbins MO (2018) Relating Chain Conformations to Extensional Stress in Entangled Polymer Melts. Physical Review Letters 121: 047801.
Palade L-I, Verney V, Attané PJRa (1996) A modified fractional model to describe the entire viscoelastic behavior of polybutadienes from flow to glassy regime. Rheologica Acta 35: 265-273.
Park SJ, Desai PS, Chen X, Larson RG (2015) Universal Relaxation Behavior of Entangled 1,4-Polybutadiene Melts in the Transition Frequency Region. Macromolecules 48: 4122-4131.
Roland CM, Archer LA, Mott PH, Sanchez-Reyes J (2004) Determining Rouse relaxation times from the dynamic modulus of entangled polymers. Journal of Rheology 48: 395-403.
Rubinstein M, Colby RH (2003) Polymer physics. Oxford University Press.
Shahid T, Clasen C, Oosterlinck F, van Ruymbeke E (2019) Diluting Entangled Polymers Affects Transient Hardening but Not Their Steady Elongational Viscosity. Macromolecules 52: 2521-2530.
Shahid T, Huang Q, Oosterlinck F, Clasen C, van Ruymbeke E (2017) Dynamic dilution exponent in monodisperse entangled polymer solutions. Soft Matter 13: 269-282.